



Article

Investigation on the Effect of a Chromium-Free Sealing Treatment for the Corrosion Resistance of AA2198-T851 after Tartaric Sulphuric Anodizing (TSA)

Fernanda Martins Queiroz ^{1,2}, Aline de Fátima Santos Bugarin ^{1,2} , Victor Hugo Ayusso ¹, Maysa Terada ^{2,*} and Isolda Costa ¹

- ¹ Energy and Nuclear Research Institute (IPEN/CNEN-SP), Av. Prof. Lineu Prestes, 2242, São Paulo 05508-000, SP, Brazil; mq_fernanda@yahoo.com.br (F.M.Q.); abugarin@usp.br (A.d.F.S.B.); imi.victor@gmail.com (V.H.A.); icosta@ipen.br (I.C.)
- ² SENAI Innovation Institute of Advanced Manufacturing and Microfabrication, Rua Bento Branco de Andrade Filho, 379, São Paulo 04757-000, SP, Brazil
- * Correspondence: maysaterada@uol.com.br

Abstract: The AA 2198-T851 is a third-generation Al-Li alloy developed for use in the aircraft industry. Al-Li alloys are susceptible to localized corrosion due to their complex microstructure resulting from the used thermomechanical treatment. In order to prevent localized corrosion, these alloys are usually protected by anodizing in order to avoid a corrosive environment. Subsequently, for anodizing, a sealing treatment is usually performed for parts. Some sealing treatments use hexavalent-chromium-containing solutions. In this investigation, a chromium-free sealing treatment in a solution with cerium ions has been carried out, and the effect on the corrosion resistance of the AA2198-T851 alloy was investigated. Hydrothermally sealed or unsealed samples were also tested for corrosion resistance for comparison reasons. The corrosion resistance of the anodized aluminum alloy, either hydrothermally sealed or in a cerium-ion-containing solution, was evaluated in a sodium chloride solution by electrochemical impedance spectroscopy as a function of immersion time. The samples sealed in a cerium-containing solution increased their corrosion resistance when compared to the hydrothermally sealed. The effectiveness of the sealing process with cerium that was observed in the electrochemical tests indicated that after the corrosive attack of the barrier layer, there was a “sealing” process of the sample surface.

Keywords: AA2198-T851; tartaric sulfuric anodizing; Ce ions; hydrothermal treatment



Citation: Queiroz, F.M.; de Fátima Santos Bugarin, A.; Ayusso, V.H.; Terada, M.; Costa, I. Investigation on the Effect of a Chromium-Free Sealing Treatment for the Corrosion Resistance of AA2198-T851 after Tartaric Sulphuric Anodizing (TSA). *Corros. Mater. Degrad.* **2023**, *4*, 331–344. <https://doi.org/10.3390/cmd4020017>

Academic Editor: Kevin Ogle

Received: 3 May 2023

Revised: 1 June 2023

Accepted: 7 June 2023

Published: 12 June 2023



Copyright: © 2023 by the authors. Licensee MDPI, Basel, Switzerland. This article is an open access article distributed under the terms and conditions of the Creative Commons Attribution (CC BY) license (<https://creativecommons.org/licenses/by/4.0/>).

1. Introduction

The increasing requirement for materials with high strength and low density for aerospace applications has led to a substantial interest in Al-Li alloys. Since aluminum is a light metal, there are a small number of alloying elements which could be used to obtain weight reduction. Among the alloying elements of lower density than Al (Si, Be, Mg, and Li), only Mg and Li present high solubility in Al (higher than 10%) [1]. Aluminum alloys containing magnesium (Mg), such as AA2024-T3, present high localized corrosion susceptibility [2]. The authors still state that Al-Cu-Mg (S-phase) IMSSs become cathodic due to the selective corrosion of Al and Mg leaving nobler Cu-rich remnants that provoke the corrosion of the adjacent matrix accelerating localized corrosion [2]. Al-Li alloys are still susceptible to localized corrosion due to the high reactivity of the Li and the resultant Li-containing phases of Al-Li alloys [2,3]. Initially, the anodic T1 phase, with respect to the matrix, undergoes selective corrosion of Li and Al leading to Cu-rich remnant and severe localized corrosion [4]. Lithium presents high solubility at high temperatures, yet aging treatments of Al-Li alloys lead to fine precipitates, increasing the strength and hardness of these alloys [5]. For instance, the addition of 1 wt% of Li in an aluminum alloy increases

its elasticity modulus by 6% and reduces density by about 3% [6,7]. However, Al-Cu-Li and Al-Cu-Mg alloys are susceptible to localized corrosion as Li and Mg are extremely reactive elements, and their presence in Al alloys favors local de-alloying, generating unstable Cu-rich clusters. Moreover, the presence of Mg slightly decreases the intergranular corrosion resistance.

The interest in the potential properties of Al-Li alloys appeared in the 1950s when the first generation of Al-Li alloys was used in specialized applications due to their cracking susceptibility [8,9]. The second generation of these alloys tried to overcome this problem by changing the alloy composition and thermomechanical processing. Despite the improvements in the second generation of Al-Li alloys, they still presented reasonably high corrosion rates and localized corrosion [10].

The third generation of Al-Li alloys was mainly developed for military and space applications with lower Li than Cu levels being designated as 2xxx alloys. The aim of this generation was to meet the demands of future commercial airframes. This generation has been increasing interest in aerospace applications due to their remarkable lightweight leading to their use in some modern aircraft [11–13]. The latest generations of commercial aircraft have been increasing the use of Al-Cu-Li alloys, mainly in applications requiring high specific strength and excellent damage tolerance [10]. The mechanical properties of Al-Li alloys have been largely investigated. The microstructure and crystallographic texture of these alloys can be controlled in order to improve not only their mechanical behavior [5,14,15] but also their damage tolerance [5,6,14,16–19].

The literature reports some Al-Li alloys, such as Al-Li-Zr and Al-Mg-Li-Zr alloys, that are more resistant to stress corrosion than most conventional alloys subjected to the same heat treatments [20]. The literature also reports the slightly lower corrosion resistance of AA2198-T851 when compared to AA2524-T3, suggesting the former as a potential replacement for the latter [17]. However, the susceptibility to localized corrosion has been lately associated with Al-Cu-Li alloys [21–25]. In order to prevent localized corrosion, anodizing processes have been studied trying to diminish their exposure to corrosive environments [26–31]. Subsequently, following anodizing, the components intended for use without coatings are hydrothermally sealed or sealed in a hexavalent-chromium-containing solution. Due to environmental constraints, treatments involving the use of hexavalent chromium ions are being increasingly banned [25].

The literature reports positive results related to TSA anodized aluminum alloys sealed with a solution containing cerium ions, obtained with electrochemical impedance spectroscopy technique as a function of immersion time in a sodium chloride solution [26–29,32]. In a study of AA2524-T3 TSA alloy anodized and partially sealed with a cerium-containing solution, corrosion resistance recovery was observed, indicating self-healing properties [31]. An investigation of partial sealing of the AA2024-T3 alloy followed by the application of a sol-gel coating indicated that the presence of Ce III ions causes self-healing without preventing the protection attributed to the sol-gel-boehmite layer [30]. Finally, the addition of peroxide to the cerium sealing solution was evaluated for Alclad 2024, indicating the incorporation of these ions into the pores of the anodized layer and increasing the corrosion resistance [32].

In this investigation, a chromium-free sealing treatment was proposed and carried out using a sulfuric-tartaric acid process (TSA). The effect on the corrosion resistance of AA2198-T851 was investigated. Hydrothermally-sealed or cerium-containing solution-sealed samples were evaluated by electrochemical impedance spectroscopy (EIS) as a function of immersion time in a sodium chloride solution.

2. Materials and Methods

AA2198-T851 produced by Constellium and provided as 1.6 mm sheets without any cladding was analyzed by Arcos optical emission spectroscopy (Spectro Analytical Instruments GmbH, Chemical Department, University of São Paulo, São Paulo, Brazil), and the chemical composition is shown in Table 1.

Table 1. Chemical composition (wt%) of the AA2198-T851 used in this study.

Elements	Cu	Mg	Li	Si	Fe	Ti	Zr	Zn	Al
AA2198-T851	3.68	0.31	1.01	0.03	0.08	0.027	0.12	0.01	Balance

Samples of 5.0 cm × 7.0 cm × 0.126 cm were degreased by sonication in acetone for 10 min and immersed in a commercial alkaline degreasing bath (Turco[®] 4215 NCLT, Henkel AG & Co. KGaA (Dusseldorf, Germany)) at 50 °C for 10 min. In addition, the samples were dipped in an alkaline etching bath (NaOH solution, 40 g·L⁻¹) at 40 °C for 30 s and in a chromate-free commercial acid dismuting bath (Turco[®] Smuttgo, Henkel AG & Co KGaA), at room temperature for 15 s. Between each step, these samples were rinsed in deionized water. The anodizing process was performed in a tartaric sulfuric acid bath (TSA) composed of 40 g·L⁻¹ H₂SO₄ + 80 g·L⁻¹ C₄H₆O₆ at a constant voltage of 14 V for 20 min at 37 °C. After anodizing, some of the samples were hydrothermally sealed, either in water at 96 °C or in a stirring solution of 50 mM of hydrated cerium nitrate at 96 °C. The sealing treatment was carried out for 25 min. The samples were positioned vertically. The anodized surface exposed to the electrolyte was 1.0 cm². Visual observation of corrosion development on the TSA anodized surface as a function of immersion time to the electrolyte was also carried out.

The corrosion resistance of these anodized and sealed samples was evaluated in naturally aerated 0.5 mol·L⁻¹ NaCl solution at (22 ± 1) °C by EIS test as a function of exposure time. Unsealed samples were also tested for comparison reasons.

A PCI4/300 potentiostat-frequency response analyzer system (Gamry, Energy and Nuclear Research Institute) was used to evaluate the corrosion resistance of the samples. EIS was carried out in a classical three electrodes arrangement using a 1.00 cm² area of the specimen as the working electrode, Ag/AgCl (+0.197 V vs. SHE) as the reference electrode, and a platinum plate as the counter electrode. EIS measurements were taken at different immersion times at room temperature in a naturally aerated 0.5 mol·L⁻¹ NaCl solution, over a frequency range from 10⁵ to 10⁻² Hz with 10 points per decade using an AC signal amplitude of 20 mV (rms). The monitoring of the electrochemical behavior during the immersion test was carried out for up to 72 h.

Scanning electron microscopy characterization was performed in a Field Emission Gun Microscope Quanta 650 (FEI, Brazilian Nanotechnology National Laboratory, Campinas, SP, Brazil).

3. Results

Figure 1 shows scanning electron microscopy (SEM) micrographs of the cross-section and from the top surface of the anodized and unsealed AA2198-T851. Figure 1A–C show, respectively, the anodic layer at lower magnifications displaying some depression in the film, a homogeneous distribution of pores in the anodic film at higher magnification, and the cross section of the layer on the AA2198-T851 supporting the presence of areas of lower thickness (seen as depression on the top view). The thickness of the anodized layer was estimated as (2.71 ± 0.56) μm, in good agreement with the literature [33–35].

Figure 2 presents SEM micrographs of the anodized hydrothermally sealed surface. The surface is covered by pseudoboehmite or boehmite (AlOOH) produced during the sealing carried out for 25 min.

Figure 3 shows the surface hydrothermally sealed in a cerium-containing solution. The layers of smudges are similar to the ones shown in Figure 2. However, a high amount of cerium oxide can be noticed on the surface in white areas, indicated by the arrows—Figure 3A,B (around 40% wt, in comparison with the 2% wt found in most parts of the surface). Figure 3C,D show two representative EDX analyses, the first one at a random area and the second at one of the white areas, indicated by the arrows in Figure 3A. The distribution and the size of these white areas on the surface of the Zr samples suggest they are

located on the flaws of the oxide layer. The cracks all over the surface could be explained by residual tension during the drying process and the precipitation of cerium hydroxide.

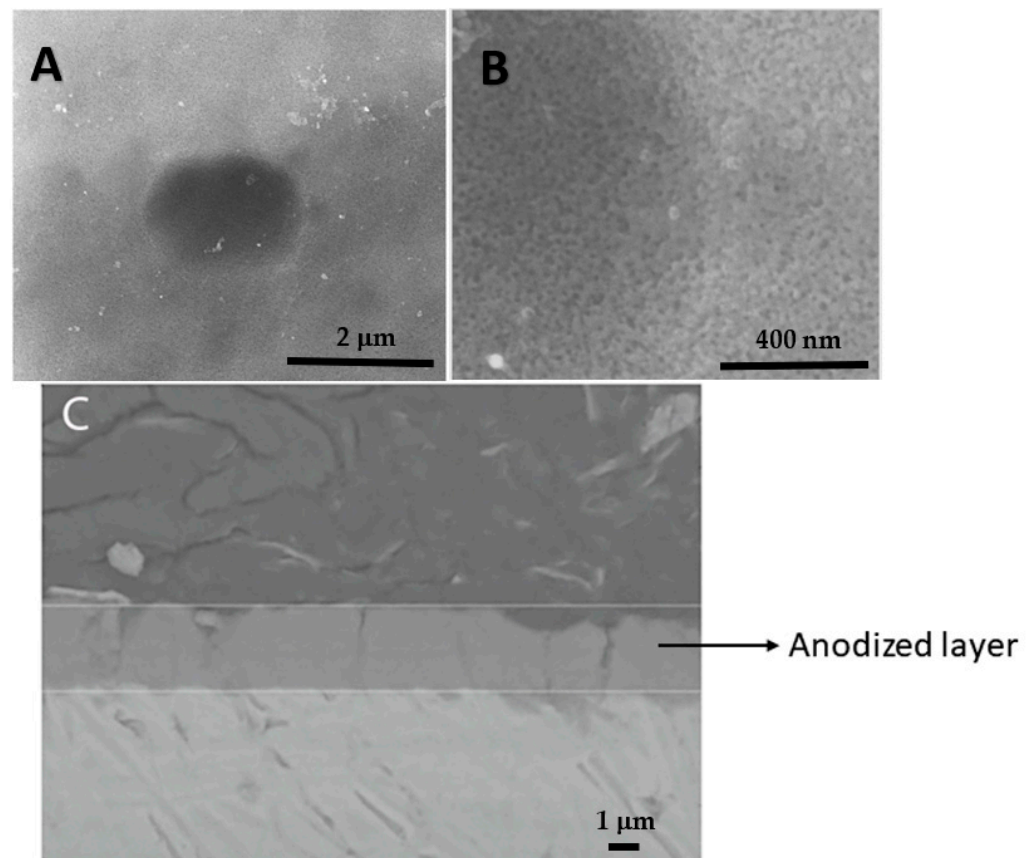


Figure 1. SEM micrographs of the anodized and unsealed AA2198-T851. (A) Top view, (B) same as (A) at higher magnifications, and (C) cross-section showing the anodic film thickness.

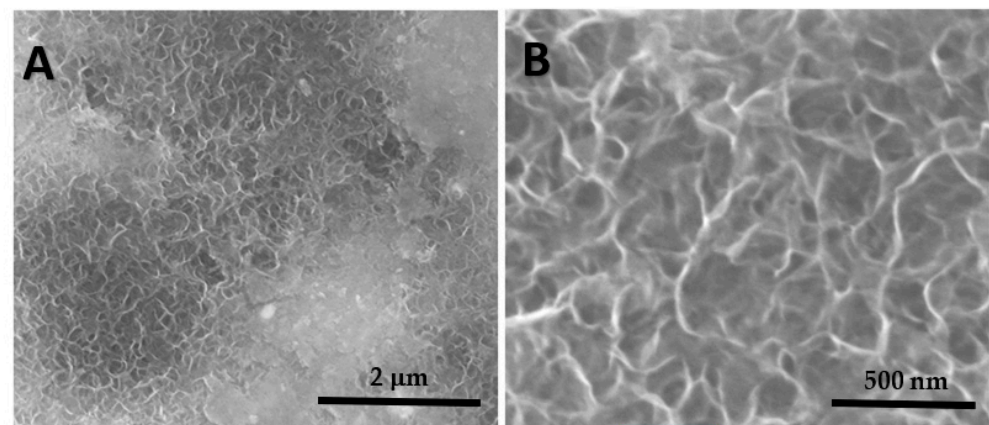


Figure 2. SEM micrographs of the AA2198-T851 surface anodized and hydrothermally sealed (B), same as (A) at higher magnifications.

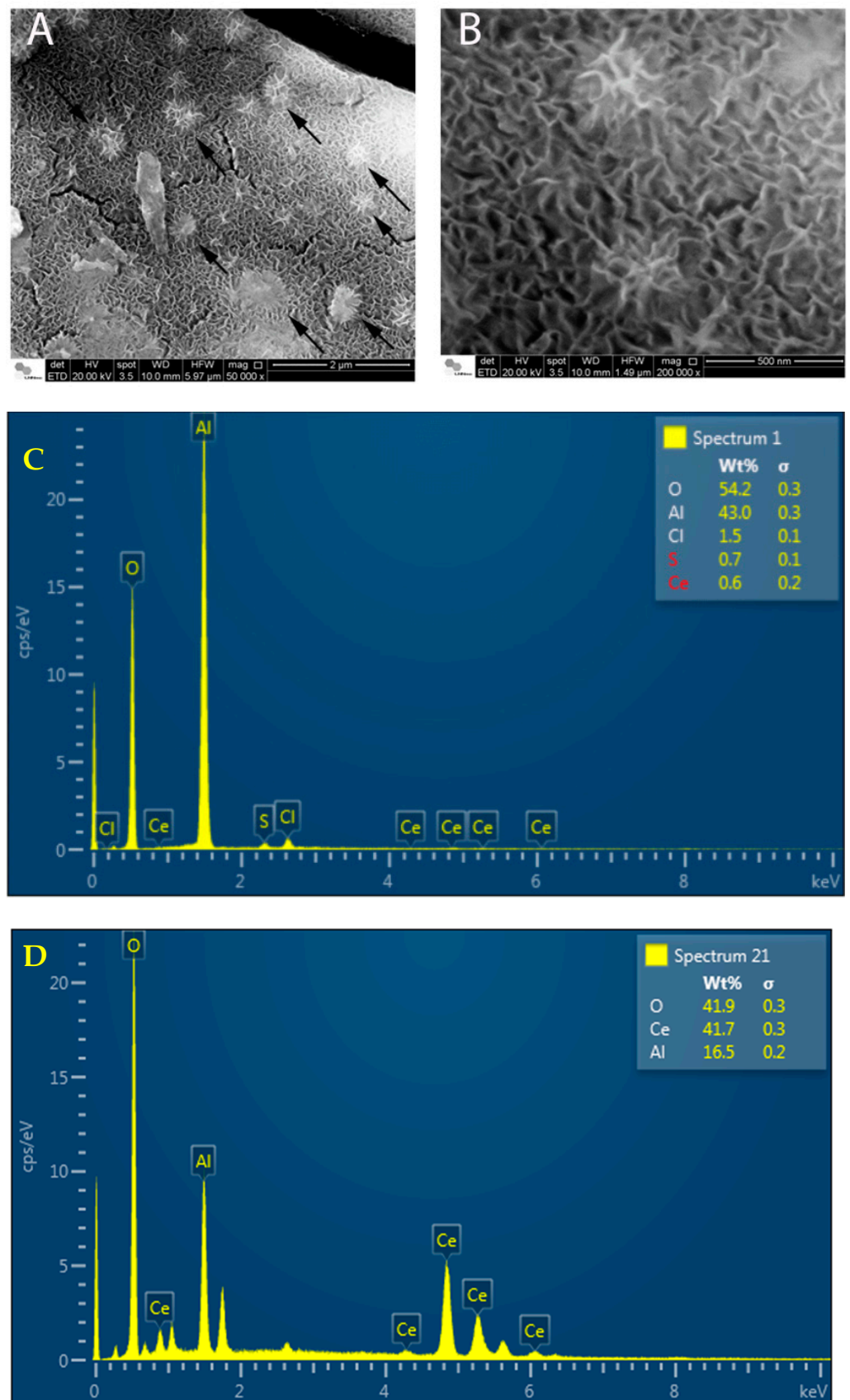


Figure 3. SEM micrographs of the AA2198-851 anodized and sealed in cerium-containing solution (**B**), same as (**A**) at higher magnifications; (**C**) representative EDX analysis performed at a random area and (**D**) EDX analysis performed at one of the white areas indicated by the arrows.

The electrochemical behavior of anodized and unsealed samples as a function of immersion time in $0.5 \text{ mol}\cdot\text{L}^{-1}$ NaCl solution was carried out by electrochemical impedance spectroscopy, and Figure 4 shows these results: Nyquist plots for 24 h, 48 h, 72 h, and 96 h, all of them presenting two-time constants. The time constant at higher frequencies is related to the unsealed porous layer, and the one at lower frequencies to the barrier layer. Figure 4 also presents an equivalent electric circuit (EEC) proposed to fit the experimental data of the anodized and unsealed AA2198-T851. Constant phase elements (CPE)—instead of pure capacitances (C)—were used to simulate the experimental data in order to consider the non-homogeneous structure of the layers. R_p and its associated CPE_p correspond to the electrolyte resistance through the porous layer. A resistance R_b and a capacitance CPE_b describe the barrier layer, which is the main aspect responsible for the corrosion resistance of the system [32,36–39].

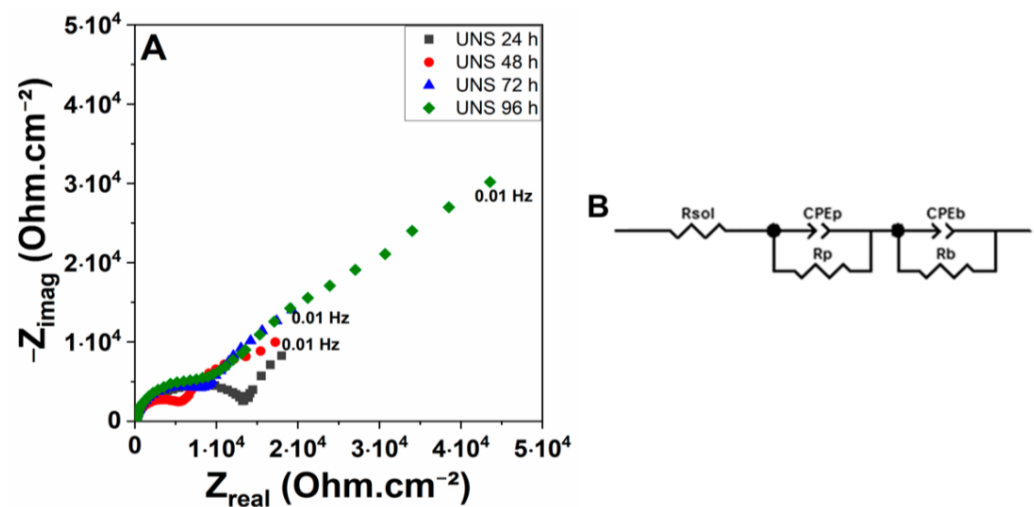


Figure 4. EIS results for the anodized and unsealed AA2198-T851 as a function of exposure time to $0.5 \text{ mol}\cdot\text{L}^{-1}$ NaCl electrolyte. (A) Nyquist diagram and (B) equivalent electric circuit proposed to fit the experimental data.

Table 2 presents the values of EEC components obtained from fitting the experimental data to the EEC proposed for the anodized and unsealed AA2198-T851 alloy exposed to the $0.5 \text{ mol}\cdot\text{L}^{-1}$ naturally aerated NaCl solution for 24, 48, 72, and 96 h.

Table 2. Values of EEC components obtained from fitting the experimental data to the EEC proposed in Figure 4 for the anodized and unsealed AA2198-T851 alloy exposed to the $0.5 \text{ mol}\cdot\text{L}^{-1}$ naturally aerated NaCl solution for 24, 48, 72, and 96 h.

AA2198-T851 Unsealed								
24 h		48 h		72 h		96 h		
		Error (%)		Error (%)		Error (%)		Error (%)
R_{sol} ($\Omega\cdot\text{cm}^2$)	25.21	-	27.68	-	25.11	-	50.39	-
CPE_p ($\text{F}/\text{cm}^2\cdot\text{s}^{a-1}$)	1.33×10^{-5}	2.2	2.39×10^{-5}	0.7	2.44×10^{-5}	1.3	1.69×10^{-5}	1.7
α_p	0.82	0.4	0.88	0.3	0.89	0.6	0.92	0.7
R_p ($\Omega\cdot\text{cm}^2$)	1.28×10^4	1.4	5.50×10^3	1.3	8.23×10^3	1.9	7.57×10^3	2.1

Table 2. Cont.

AA2198-T851 Unsealed								
	24 h		48 h		72 h		96 h	
	Error (%)		Error (%)		Error (%)		Error (%)	
CPE_b ($F/cm^2 \cdot s^{n-1}$)	1.46×10^{-3}	6.4	3.83×10^{-4}	2.3	3.40×10^{-4}	3.3	1.13×10^{-4}	1.6
α_b	1.0	-	0.78	1.4	0.73	1.7	0.72	0.7
R_b ($\Omega \cdot cm^2$)	1.44×10^4	11.7	2.72×10^4	3.3	7.66×10^4	10.4	8.45×10^4	2.9

Figure 5A,B show the Nyquist and equivalent electric circuit proposed to fit the experimental data of the AA2198-T851 anodized and hydrothermally sealed exposed to $0.5 \text{ mol} \cdot \text{L}^{-1}$ NaCl solution at various exposure periods (24 h, 48 h, 72 h, and 96 h). Up to 48 h of immersion, the surface was stable.

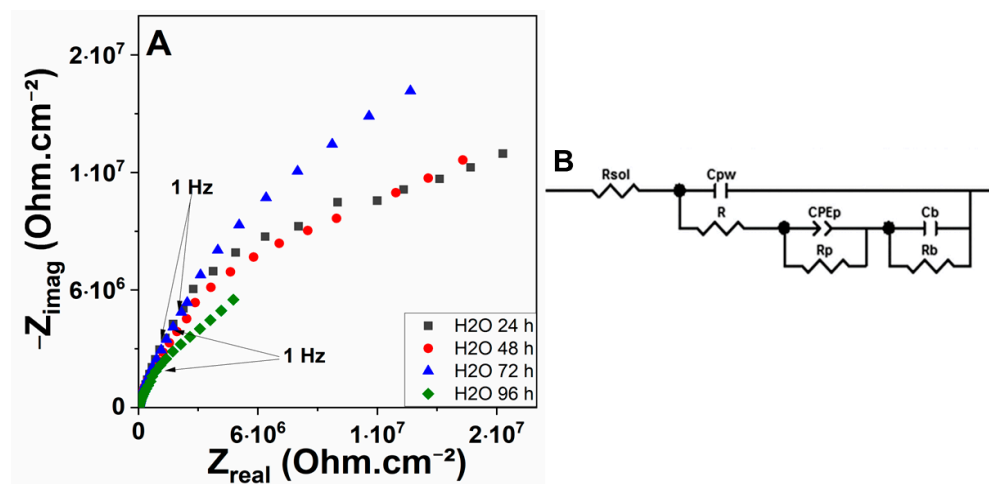


Figure 5. EIS results for the AA2198-T851 anodized and hydrothermally sealed in $0.5 \text{ mol} \cdot \text{L}^{-1}$ NaCl solution as a function of exposure time (A) Nyquist diagram and (B) equivalent electric circuit proposed to fit the experimental data.

Figure 6A,B show the electrochemical impedance spectroscopy results and equivalent electric circuit proposed to fit the experimental data of the AA2198-T851 anodized and sealed in cerium-containing solution exposed to $0.5 \text{ mol} \cdot \text{L}^{-1}$ NaCl solution as a function of exposure time (24 h, 48 h, 72 h, and 96 h). It is interesting to notice the impedance oscillations for this surface. For instance, EIS impedance values increased between 24 h and 48 h of immersion, decreased between 48 h and 72 h, and increased again between 72 h and 96 h of the test. This behavior was highly reproducible and might be explained by a “self-healing” effect of the precipitation of cerium hydroxide partially blocking the corroding areas due to the attack of aggressive species in the electrolyte. The impedance associated with this surface is always superior to that related to hydrothermally sealed surfaces even at the initial periods of immersion indicating the protection of the anodized layer occurs even during the sealing treatment in this solution. The similarity of curves corresponding to 24 h and 72 h and those related to the results for 48 h and 96 h suggests the complete recovery of the protective properties of the anodized layer after its attack by the electrolyte.

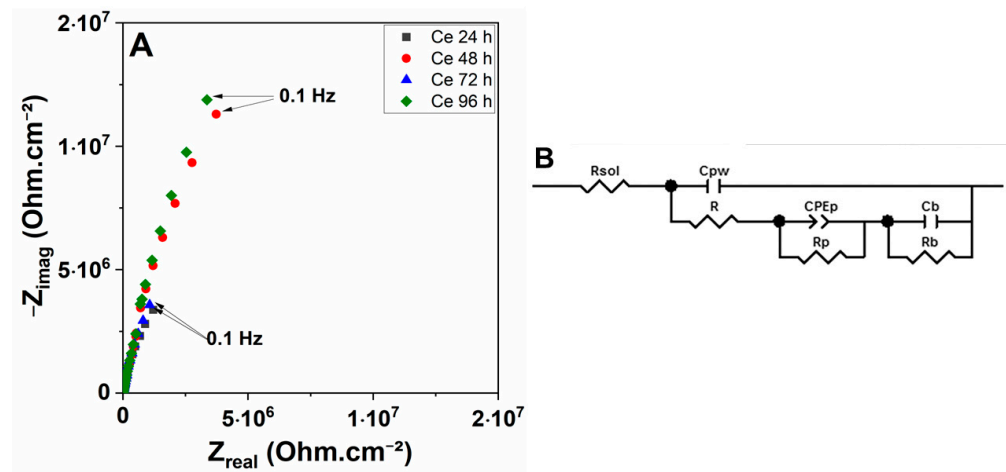


Figure 6. EIS results for the AA2198-T851 anodized and sealed in cerium-containing solution as a function of exposure time to $0.5 \text{ mol}\cdot\text{L}^{-1}$ NaCl solution. (A) Nyquist diagram and (B) equivalent electric circuit proposed to fit the experimental data.

Tables 3 and 4 present values obtained from fitting the data to the EEC components, composed of three time constants. In this circuit, the porous layer is characterized by the electrolyte resistance through the pores R_p and its associated CPE_p . A resistance R_b and a capacitance C_b also describe the barrier layer which is the main aspect responsible for the corrosion resistance of the system. The use of a pure capacitor to describe the pore walls (C_{pw}) and the barrier layer suggests that the systems are homogeneous and free of defects. The use of a pure capacitor instead of a CPE was due to the proximity of the α value to 1. A third resistance (R) appears in parallel with C_{pw} and in series with $CPE_p // R_p$ and $C_b // R_b$. This R is lower than $600 \Omega\cdot\text{cm}^2$ in both cases and can be related to the electrolyte in the pores and the defects of an intermediate layer, as has been proposed in the literature [22,23,25,35].

Table 3. EEC components values obtained from fitting the experimental data to the model proposed and shown in Figure 5 for the AA2198-T851 alloy when anodized, sealed in hot water, and exposed to $0.5 \text{ mol}\cdot\text{L}^{-1}$ naturally aerated NaCl solution for 24 h, 48 h, 72 h, and 96 h.

AA2198-T851 Alloy Anodized and Sealed in Hot Water								
	24 h		48 h		72 h		96 h	
		Error (%)		Error (%)		Error (%)		Error (%)
R_{sol} ($\Omega\cdot\text{cm}^2$)	61.82	7.2	62.82	13.4	100.1	4.5	80.65	5.2
C_{pw} (F/cm^2)	1.91×10^{-8}	7.2	1.77×10^{-8}	12.4	1.62×10^{-8}	5.4	1.50×10^{-8}	4.2
R ($\Omega\cdot\text{cm}^2$)	150.6	2.4	164.6	4.2	208.7	1.9	255.8	1.7
CPE_p ($\text{F}/\text{cm}^2\cdot\text{s}^{\alpha-1}$)	7.86×10^{-7}	1.1	9.09×10^{-7}	2.8	1.01×10^{-6}	1.7	9.56×10^{-7}	1.4
α_p	0.86	0.2	0.86	0.5	0.85	0.3	0.85	0.3
R_p ($\Omega\cdot\text{cm}^2$)	4.64×10^6	2.1	1.62×10^6	4.9	8.46×10^6	3.3	1.97×10^6	2.8
C_b (F/cm^2)	6.28×10^{-6}	-	2.29×10^{-6}	-	1.36×10^{-6}	-	1.95×10^{-6}	-
R_b ($\Omega\cdot\text{cm}^2$)	5.88×10^6	17.7	5.71×10^6	6.9	8.63×10^6	3.2	1.14×10^7	4.3

Table 4. EEC components values obtained from fitting the experimental data to the model proposed and shown in Figure 6 for the AA2198-T851 alloy anodized, sealed in cerium-ion-containing solution, and exposed to $0.5 \text{ mol}\cdot\text{L}^{-1}$ naturally aerated NaCl solution for 24 h, 48 h, 72 h, and 96 h.

AA2198-T851 Alloy Anodized and Sealed in Solution with Cerium Ions								
	24 h		48 h		72 h		96 h	
	Error (%)		Error (%)		Error (%)		Error (%)	
R_{sol} ($\Omega\cdot\text{cm}^2$)	28.08	-	125.4	-	33.2	-	141.5	5.2
Cp_w (F/cm^2)	4.44×10^{-8}	2.0	1.37×10^{-7}	1.9	3.55×10^{-8}	2.0	1.17×10^{-8}	4.1
R ($\Omega\cdot\text{cm}^2$)	80.96	1.3	367.1	1.4	139.7	1.5	520.0	2.2
CPE_p ($\text{F}/\text{cm}^2\cdot\text{s}^{a-1}$)	3.89×10^{-6}	2.4	1.51×10^{-6}	2.6	4.04×10^{-6}	3.5	1.08×10^{-6}	3.1
α_p	0.85	0.4	0.85	0.4	0.84	0.6	0.85	0.6
R_p ($\Omega\cdot\text{cm}^2$)	2.31×10^5	8.1	8.33×10^5	8.7	2.29×10^5	13.1	2.59×10^6	9.7
C_b (F/cm^2)	2.10×10^{-6}	1.2	6.39×10^{-7}	1.3	1.99×10^{-6}	1.9	6.94×10^{-7}	-
R_b ($\Omega\cdot\text{cm}^2$)	1.31×10^7	3.5	4.89×10^7	4.3	1.48×10^7	10.0	8.64×10^7	13.4

After the electrochemical tests, TSA-anodized and sealed AA2198-T851 samples were analyzed using SEM—Figure 7. Figure 7A,B show some corrosion products on the surface of the hydrothermally sealed samples, despite the high R_p and R_b values obtained by EIS fittings. On the other hand, Figure 7C,D show the absence of corroded areas and the similarity of the smudges of the cerium-containing sealed samples with Figure 3, indicating that the cerium improved the corrosion resistance of these samples.

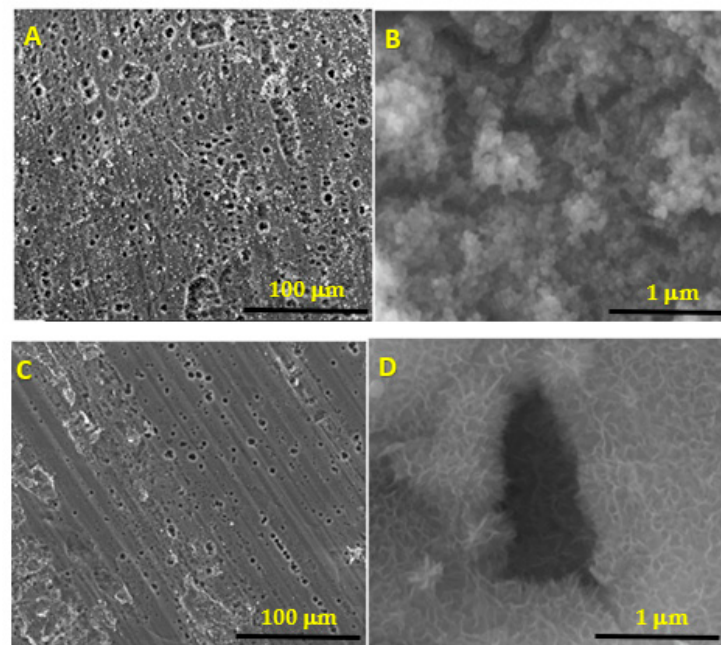


Figure 7. Micrographs of the TSA anodized and sealed AA2198-T851 surface after 96 h of immersion in $0.5 \text{ mol}\cdot\text{L}^{-1}$ NaCl solution. (A) hydrothermally sealed, (B) same as (A), at higher magnification, (C) sealed in cerium ions containing solution, and (D) same as (C), at higher magnifications. SE.

4. Discussion

Figure 8A,B present the fitting data values of R_p - CPE_p components for unsealed and sealed layers of anodized AA2198-T851, respectively, in $0.5 \text{ mol}\cdot\text{L}^{-1}$ NaCl solution. The slight increase in R_p values of the unsealed anodized layers when exposed to aggressive electrolytes is associated with the progressive precipitation of hydrated alumina inside the pores during the partial sealing process [29–34]. These results show the resistance of the porous layer oscillating with the time of immersion for the sealed samples. It also indicates the protective effect of the sealing treatment in cerium-ion-containing solution in the first days of immersion is not related to the protective properties of the porous layer. At 96 h of immersion, the R_p values of both sealed samples are similar although slightly higher than the sample sealed in the cerium-containing solution, indicating the increasing resistance of this sealing treatment with the time of exposure. This was likely due to partial blockage of the pores by the precipitation of cerium hydroxide at the regions surrounding the corroding areas caused by the attack of the environment-aggressive species. The oscillation of CPE_p values with the time of exposure for the anodized alloy sealed in cerium-containing solution in comparison with a more stable behavior for the hydrothermally sealed alloy (Figure 8) indicates the higher complexity of the first type of oxide layer. In fact, the anodic layers resulting from sealing in the cerium-containing solution presented cracks that were not seen on the hydrothermally sealed samples.

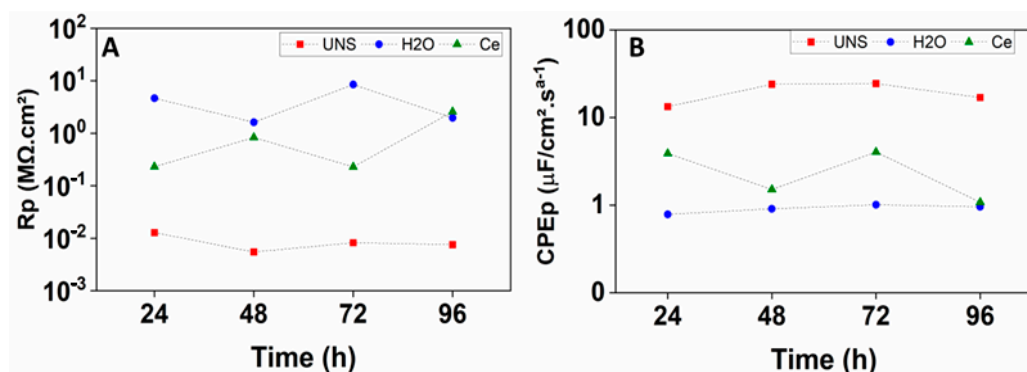


Figure 8. Variation of the (A) R_p and (B) CPE_p component values as a function of the exposure time to NaCl $0.5 \text{ mol}\cdot\text{L}^{-1}$ solution.

For the barrier layer, the results in Figure 9 show the highest impedances, associated with the layer sealed in the cerium-containing solution due to the modification in this layer. Oscillations in the values of R_b with time were detected due to the reaction of the anhydrous alumina with adsorbed water leading to voluminous hydrated alumina resulting in a self-sealing effect and an increase in the resistance of the porous layer. Despite the self-sealing effect with time and the penetration of the corrosive environment, gradual deterioration of the barrier layer arises, leading to a decrease in the R_b . However, each decrease in R_b was followed by a subsequent increase in the aluminum alloy sealed in a cerium-containing solution and there was a trend of R_b increasing with time. This “healing” effect might have been caused by cerium hydroxide precipitation due to the presence of cerium ions in the barrier layer in the neighborhood of the corroding areas. This precipitation at the base of the pores explains the combined effects found on both the porous and barrier layers. According to the literature, the self-sealing mechanism involves degradation, gelling, agglomeration, and a precipitation process [23–26]. The CPE_b and C_b values slowly decrease as the hydration process progresses and might lead to the decreased homogeneity of the barrier layer.

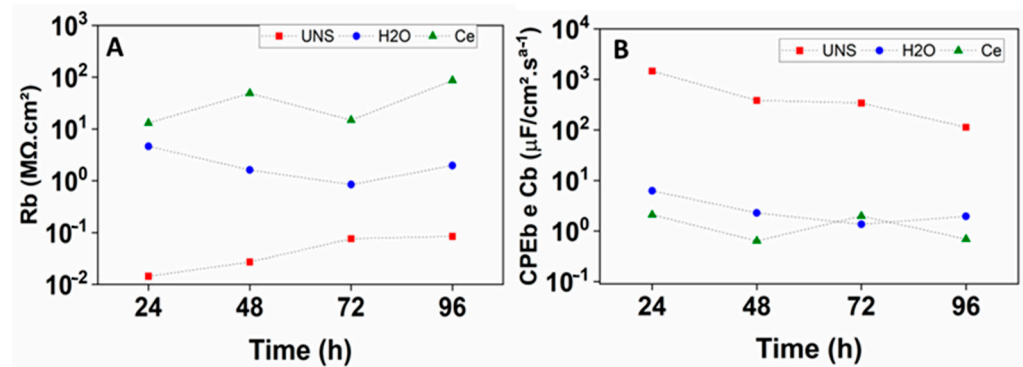


Figure 9. Variation of the (A) R_b , (B) CPE_b , and C_b component values as a function of the exposure time to NaCl 0.5 mol·L⁻¹ solution.

The variations of the α_p parameter with time—Figure 10—take into consideration the non-ideal capacitive behavior of porous layers. In aqueous environments, unsealed films are subjected to self-sealing caused by the hydration process leading to a decrease in defects in the porous layer. The aging of unsealed anodic films improves sealing quality. However, at the same time, due to the absorbing properties of the unsealed layers, a gradual deterioration of the barrier layer caused by corrosion decreased the α_b values as indicated in Figure 11. This parameter is close to 1 at the first hours of immersion indicating the homogeneity and the low number of defects in the barrier layer.

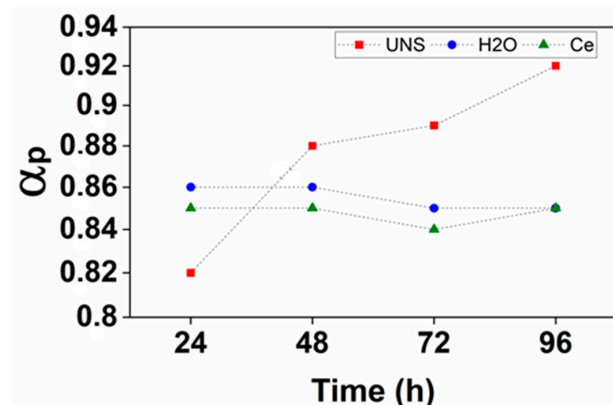


Figure 10. Variation in the α_p component values as a function of the exposure time to NaCl 0.5 mol·L⁻¹ solution.

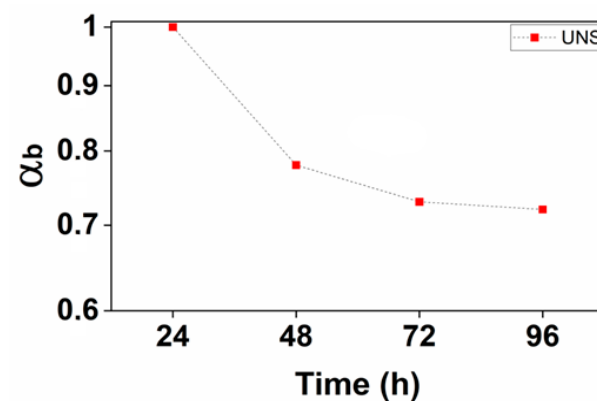


Figure 11. Variation in the α_b component values as a function of the exposure time to NaCl 0.5 mol·L⁻¹ solution.

Figure 12A,B show the R_w - CPE_w values' variation with the time of exposure to the electrolyte. The pair R_w - CPE_w is assumed to represent the response of the pore walls. The resistance of the pore walls of the sealed samples in cerium-containing solution was initially lower than hydrothermally sealed ones. However, the resistance associated with the former oscillated with time, whereas it slowly increased for the latter. Nonetheless, the CPE_w values for the cerium-sealed samples were initially significantly superior to the hydrothermally sealed ones, but it largely decreased after 48 h of exposure, and at the end of the test (96 h), it was slightly lower. This is supposedly related to the cracked characteristics of the anodic layer on the anodized samples sealed in cerium-containing solutions and the increased blockage of the cracks by the hydrated and precipitated products leading to the filling of the cracks in these products.

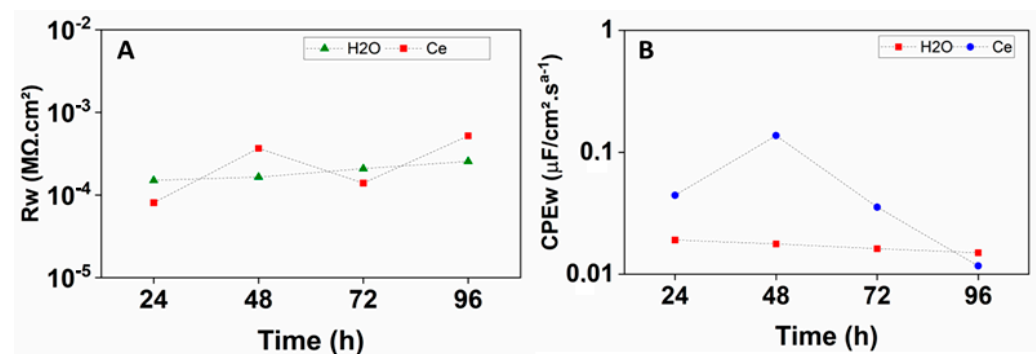


Figure 12. Variation in the (A) R_w and (B) CPE_w values for AA2198-T851 alloy anodized and sealed as a function of exposure time to NaCl $0.5 \text{ mol} \cdot \text{L}^{-1}$ solution.

Figure 13 presents the Bode IZI diagram comparing all the results from EIS tests. The cerium effect at lower frequencies is evident as the impedance value of these sealed samples in cerium solution increased by two orders of magnitude in comparison with the hydrothermally sealed samples.

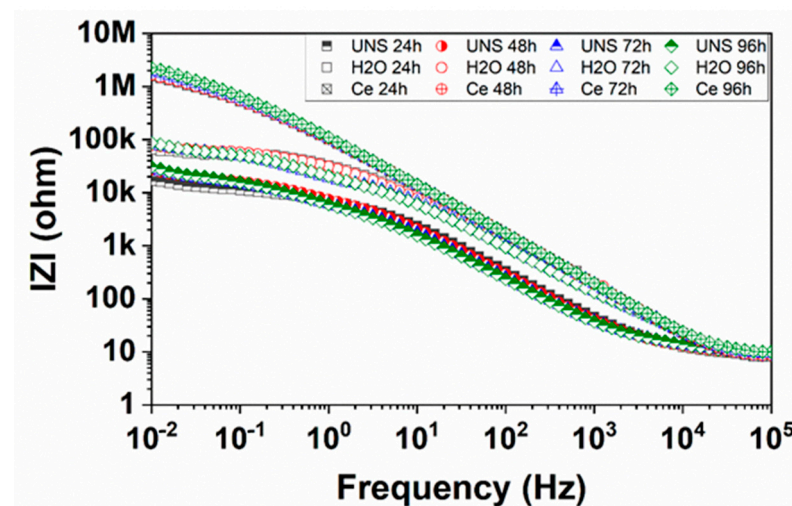


Figure 13. Bode IZI comparing all the results obtained from EIS tests. UNS represents the unsealed samples; H₂O, the hydrothermally sealed samples; and Ce, the samples sealed in Ce solution.

5. Conclusions

The sealing procedure proved to be efficient in the process of the incorporation of Ce into the anodic layer pores. The results indicated an increase in the corrosion resistance of the anodized AA2198-T851 sealed in a cerium-containing solution when compared to the hydrothermal sealing. The EIS suggested a sealing process following the corrosive attack of the barrier layer for the samples sealed in the cerium-containing solution. The sealing,

associated with a healing effect, was achieved by cerium hydroxide precipitation due to the presence of cerium ions in the barrier layer around the corroding areas, indicating the effectiveness of the sealing process.

Author Contributions: Methodology, F.M.Q., V.H.A., M.T.; validation, F.M.Q.; formal analysis, V.H.A., M.T.; investigation, F.M.Q., M.T.; data curation, F.M.Q.; writing—original draft preparation, F.M.Q., A.d.F.S.B., M.T.; writing—review and editing, F.M.Q., A.d.F.S.B., M.T.; visualization, F.M.Q., A.d.F.S.B.; supervision, I.C.; project administration, I.C. All authors have read and agreed to the published version of the manuscript.

Funding: This research was funded by CNPq grant number 400781/2013-1 and 48-141/2012-6 and CAPES grant number 1536157.

Acknowledgments: The authors are thankful to EML/LNNano for scanning electron microscopy images.

Conflicts of Interest: The authors declare no conflict of interest.

References

1. MacKenzie, D.S.; Totten, G.E. *Handbook of Aluminum*, 1st ed.; Totten, G.E., MacKenzie, D.S., Eds.; CRC Press: Boca Raton, FL, USA, 2003; ISBN 9780203912607.
2. Queiroz, F.M.; Magnani, M.; Costa, I.; de Melo, H.G. Investigation of the Corrosion Behaviour of AA 2024-T3 in Low Concentrated Chloride Media. *Corros. Sci.* **2008**, *50*, 2646–2657. [[CrossRef](#)]
3. Noble, B.; Thompson, G.E. Ti (Al₂CuLi) Precipitation in Aluminium–Copper–Lithium Alloys. *Metal. Sci. J.* **1972**, *6*, 167–174. [[CrossRef](#)]
4. De Sousa Araujo, J.V.; Donatus, U.; Queiroz, F.M.; Terada, M.; Milagre, M.X.; de Alencar, M.C.; Costa, I. On the Severe Localized Corrosion Susceptibility of the AA2198-T851 Alloy. *Corros. Sci.* **2018**, *133*, 132–140. [[CrossRef](#)]
5. Hatamleh, O.; Hill, M.; Forth, S.; Garcia, D. Fatigue Crack Growth Performance of Peened Friction Stir Welded 2195 Aluminum Alloy Joints at Elevated and Cryogenic Temperatures. *Mater. Sci. Eng. A* **2009**, *519*, 61–69. [[CrossRef](#)]
6. Prasad, N.E.; Gokhale, A.A.; Rao, P.R. Mechanical Behaviour of Aluminium-Lithium Alloys. *Sadhana* **2003**, *28*, 209–246. [[CrossRef](#)]
7. Warner, T. Recently-Developed Aluminium Solutions for Aerospace Applications. *Mater. Sci. Forum.* **2006**, *519–521*, 1271–1278. [[CrossRef](#)]
8. Sanders, T.H.; Starke, E.A., Jr. Aluminum-Lithium Alloys. In Proceedings of the 2nd International Conference on Aluminum-Lithium Alloys, Monterey, CA, USA, 12 April 1983.
9. Sanders, T.H., Jr.; Starke, E.A., Jr. Aluminum-Lithium Alloys. In Proceedings of the 1st International Aluminum-Lithium Alloys, Stone Mountain, CA, USA, 1 December 1980.
10. Rioja, R.J.; Liu, J. The Evolution of Al-Li Base Products for Aerospace and Space Applications. *Metall. Mater. Trans. A Phys. Metall. Mater. Sci.* **2012**, *43*, 3325–3337. [[CrossRef](#)]
11. Garrard, W. Corrosion Behavior of Aluminum-Lithium Alloys. *Corros. Sci.* **1994**, *50*, 215–225. [[CrossRef](#)]
12. Semenov, A.M. Effect of Mg Additions and Thermal Treatment on Corrosion Properties of Al-Li-Cu-Base Alloys. *Prot. Met.* **2001**, *37*, 126–131. [[CrossRef](#)]
13. Ambat, R.; Dwarakadasa, E.S. The Influence of PH on the Corrosion of Medium Strength Aerospace Alloys 8090, 2091 and 2014. *Corros. Sci.* **1992**, *33*, 681–690. [[CrossRef](#)]
14. Cavaliere, P.; Cabibbo, M.; Panella, F.; Squillace, A. 2198 Al-Li Plates Joined by Friction Stir Welding: Mechanical and Microstructural Behavior. *Mater. Des.* **2009**, *30*, 3622–3631. [[CrossRef](#)]
15. Bello, N.; Larignon, C.; Douin, J. Long-Term Thermal Ageing of the 2219-T851 and the 2050-T84 Al-Cu Alloys. *Mater. Today Commun.* **2021**, *29*, 102834. [[CrossRef](#)]
16. Bitondo, C.; Prisco, U.; Squillace, A.; Buonadonna, P.; Dionoro, G. Friction-Stir Welding of AA 2198 Butt Joints: Mechanical Characterization of the Process and of the Welds through DOE Analysis. *Int. J. Adv. Manuf. Technol.* **2011**, *53*, 505–516. [[CrossRef](#)]
17. Moreto, J.; Gamboni, O.; Rocha, L. Corrosion Behavior of Al and Al-Li Alloys Used as Aircraft Materials. *Corrosão E Proteção De Mater.* **2012**, *31*, 60–64.
18. Sepe, R.; Giannella, V.; Mazza, P.; Armentani, E.; Javad Razavi, S.M.; Berto, F. Fatigue Fracture Tests on Al-Li 2198-T851 Specimens under Mixed-Mode Conditions. In Proceedings of the Procedia Structural Integrity; Elsevier: Amsterdam, The Netherlands, 2021; Volume 39, pp. 546–551.
19. Yang, Y.; Bi, J.; Liu, H.; Li, Y.; Li, M.; Ao, S.; Luo, Z. Research Progress on the Microstructure and Mechanical Properties of Friction Stir Welded Al-Li Alloy Joints. *J. Manuf. Process.* **2022**, *82*, 230–244. [[CrossRef](#)]
20. Conde, A.; Fernández, B.J.; De Damborenea, J.J. Characterization of the SCC Behaviour of 8090 Al-Li Alloy by Means of the Slow-Strain-Rate Technique. *Corros. Sci.* **1998**, *40*, 91–102. [[CrossRef](#)]
21. Ma, Y.; Zhou, X.; Thompson, G.E.; Curioni, M.; Hashimoto, T.; Skeldon, P.; Thomson, P.; Fowles, M. Anodic Film Formation on AA 2099-T8 Aluminum Alloy in Tartaric-Sulfuric Acid. *J. Electrochem. Soc.* **2011**, *158*, C17. [[CrossRef](#)]

22. Georgoulis, D.; Charalampidou, C.M.; Alexopoulos, N.D. Corrosion Resistance of Aluminum Alloy 2198 for Different Ageing Tempers. In Proceedings of the Procedia Structural Integrity; Elsevier: Amsterdam, The Netherlands, 2021; Volume 37, pp. 941–947.
23. Ferreira, M.O.A.; Gelamo, R.V.; Marino, C.E.B.; da Silva, B.P.; Aoki, I.V.; da Luz, M.S.; Alexopoulos, N.D.; Leite, N.B.; Moreto, J.A. Effect of Niobium Oxide Thin Film on the Long-Term Immersion Corrosion of the 2198-T851 Aluminium Alloy. *Materialia* **2022**, *22*, 101407. [[CrossRef](#)]
24. Da Silva, R.M.P.; Milagre, M.X.; Izquierdo, J.; Betancor-Abreu, A.M.; de Oliveira, L.A.; de S. Araujo, J.V.; Antunes, R.A.; Souto, R.M.; Costa, I. Surface Finishing Effects on the Corrosion Behavior and Electrochemical Activity of 2098-T351 Aluminum Alloy Investigated Using Scanning Microelectrochemical Techniques. *Mater. Charact.* **2022**, *191*, 112130. [[CrossRef](#)]
25. Da Silva, R.M.P.; Izquierdo, J.; Milagre, M.X.; de S. Araujo, J.V.; Antunes, R.A.; Souto, R.M.; Costa, I. Electrochemical Characterization of Alloy Segregation in the Near-Surface Deformed Layer of Welded Zones of an Al–Cu–Li Alloy Using Scanning Electrochemical Microscopy. *Electrochim. Acta.* **2022**, *427*, 140873. [[CrossRef](#)]
26. Yu, X.; Cao, C. Electrochemical Study of the Corrosion Behavior of Ce Sealing of Anodized 2024 Aluminum Alloy. *Thin Solid. Film.* **2003**, *423*, 252–256. [[CrossRef](#)]
27. Zhao, J.M.; Chen, S.L.; Huo, P. Comparative Studies on Corrosion Behaviour of Sealed Aluminium with Cerium Salt under Bidirectional Pulse Electric Field. *Corros. Eng. Sci. Technol.* **2012**, *47*, 203–208. [[CrossRef](#)]
28. Song, D.; Ma, M.; Zhao, L. Study of Sealing of Anodized Aluminium in Mixed Titanium- Cerium Salt Solutions. *Int. J. Electrochem. Sci.* **2022**, *17*, 221224. [[CrossRef](#)]
29. Carangelo, A.; Curioni, M.; Acquesta, A.; Monetta, T.; Bellucci, F. Application of EIS to In Situ Characterization of Hydrothermal Sealing of Anodized Aluminum Alloys: Comparison between Hexavalent Chromium-Based Sealing, Hot Water Sealing and Cerium-Based Sealing. *J. Electrochem. Soc.* **2016**, *163*, C619–C626. [[CrossRef](#)]
30. Terada, M.; Queiroz, F.M.; Costenaro, H.; Ayusso, V.H.; Olivier, M.; Costa, I.; de Melo, H.G. Effect of Cerium Addition to a Hydrothermal Treatment on the Corrosion Protection of the Tartaric-Sulfuric Acid Anodized AA2524-T3. *Corrosion* **2019**, *75*, 1110–1117. [[CrossRef](#)]
31. Terada, M.; Queiroz, F.M.; Aguiar, D.B.S.; Ayusso, V.H.; Costenaro, H.; Olivier, M.-G.; de Melo, H.G.; Costa, I. Corrosion Resistance of Tartaric-Sulfuric Acid Anodized AA2024-T3 Sealed with Ce and Protected with Hybrid Sol–Gel Coating. *Surf. Coat. Technol.* **2019**, *372*, 422–426. [[CrossRef](#)]
32. Prada Ramirez, O.M.; Queiroz, F.M.; Terada, M.; Donatus, U.; Costa, I.; Olivier, M.-G.; de Melo, H.G. EIS Investigation of a Ce-Based Posttreatment Step on the Corrosion Behaviour of Alclad AA2024 Anodized in TSA. *Surf. Interface Anal.* **2019**, *51*, 1260–1275. [[CrossRef](#)]
33. Milagre, M.X.; Mogili, N.V.; Donatus, U.; Giorjão, R.A.R.; Terada, M.; Araujo, J.V.S.; Machado, C.S.C.; Costa, I. On the Microstructure Characterization of the AA2098-T351 Alloy Welded by FSW. *Mater. Charact.* **2018**, *140*, 233–246. [[CrossRef](#)]
34. De Sousa Araujo, J.V.; Santos Bugarin, A.D.F.; Donatus, U.; Machado, C.D.S.C.; Queiroz, F.M.; Terada, M.; Astarita, A.; Costa, I. Thermomechanical Treatment and Corrosion Resistance Correlation in the AA2198 Al–Cu–Li Alloy. *Corros. Eng. Sci. Technol.* **2019**, *54*, 575–586. [[CrossRef](#)]
35. Li, F.; Zhang, L.; Metzger, R.M. On the Growth of Highly Ordered Pores in Anodized Aluminum Oxide. *Chem. Mater.* **1998**, *10*, 2470–2480. [[CrossRef](#)]
36. García-Rubio, M.; de Lara, M.P.; Ocón, P.; Diekhoff, S.; Beneke, M.; Lavía, A.; García, I. Effect of Posttreatment on the Corrosion Behaviour of Tartaric-Sulphuric Anodic Films. *Electrochim. Acta* **2009**, *54*, 4789–4800. [[CrossRef](#)]
37. Ren, J.; Zuo, Y. The Anodizing Behavior of Aluminum in Malonic Acid Solution and Morphology of the Anodic Films. *Appl. Surf. Sci.* **2012**, *261*, 193–200. [[CrossRef](#)]
38. Van der Linden, B.; Terry, H.; Vereecken, J. Investigation of Anodic Aluminium Oxide Layers by Electrochemical Impedance Spectroscopy. *J. Appl. Electrochem.* **1990**, *20*, 798–803. [[CrossRef](#)]
39. Capelossi, V.R.; Poelman, M.; Recloux, I.; Hernandez, R.P.B.; de Melo, H.G.; Olivier, M.G. Corrosion Protection of Clad 2024 Aluminum Alloy Anodized in Tartaric-Sulfuric Acid Bath and Protected with Hybrid Sol–Gel Coating. *Electrochim. Acta.* **2014**, *124*, 69–79. [[CrossRef](#)]

Disclaimer/Publisher’s Note: The statements, opinions and data contained in all publications are solely those of the individual author(s) and contributor(s) and not of MDPI and/or the editor(s). MDPI and/or the editor(s) disclaim responsibility for any injury to people or property resulting from any ideas, methods, instructions or products referred to in the content.